Synthesis of Ferromagnetic Nanocomposites from Nanocrystalline Cellulose and Characterization as an Adsorbent to Remove Lead in the Water

Bao Tran Pham Ngoc[a,b], Ngoc Han Tran Thi[a,b], Thanh Son Dinh[a,b], Nhan Tu Le Tan[a,b], Nguyen Phuc Thien Le[a,b], Thanh Phong Mai[a,b], Dinh Quan Nguyen[a,b,*]

[a]Laboratory of Biofuel and Biomass Research, Faculty of Chemical Engineering, Ho Chi Minh City University of Technology (HCMUT), 268 Ly Thuong Kiet, District 10, Ho Chi Minh City, Vietnam.
[b]Vietnam National University Ho Chi Minh City, Linh Trung Ward, Thu Duc District, Ho Chi Minh City, Vietnam.
 ndquan@hcmut.edu.vn

This research presented a method to synthesize magnetic nanocrystalline cellulose-based nanocomposites using in-situ co-precipitation technique to produce ferromagnetic oxide particles (Fe_3O_4) that were grafted on the surface of cellulose nanocrystals (CNCs). The synthesized material was used to remove lead ions from aqueous solutions. Different physicochemical analyst techniques such as XRD, FTIR, SEM, and TEM were used to characterize the structure of the material upon the different ratios of cellulose nanocrystals/ Fe_3O_4. The XRD analysis showed that CNC/Fe_3O_4 nanocomposite has characteristic diffraction peaks corresponding to Fe_3O_4 and cellulose nanocrystals. The FTIR spectrum indicated the specific functional groups of Fe_3O_4 and CNC in the nanocomposite materials. The size of nanoparticles produced in this work were less than 15 nm with Fe_3O_4 and roughly 25 nm with CNC via image SEM and TEM. According to these studies, with the same Pb^{2+} concentration in water of 200 ppm, the best condition for homogenous materials was the 1:1 ratio (cellulose nanocrystals: Fe_3O_4) and the absorption capacity at time balance (q_e) was 0.1132 mg/g. The lead adsorption of material was evaluated by the ICP-OES measurement method. The equilibrium data fitted the Freundlich isotherm model better than the Langmuir isotherm model. The new adsorbent can help removing 60 % of Pb^{2+} from the solution and can be magnetically separated from the continuous phase.

1. Introduction

Cellulose was a widely used renewable material that was becoming more and more popular nowadays. With properties such as low density, biocompatibility, non-toxicity, biodegradability, low coefficient of thermal expansion, large surface area, high specific strength, and high modulus (Khalil et al., 2012), cellulose at nanometric scale (nano cellulose) was considered as a renewable nanomaterial for the application of sustainable, high-performance materials. Nanocellulose was divided into three primary types based on morphological properties, consisting of cellulose nanocrystals (CNCs), cellulose nanofibrils (CNFs), and bacterial nanocellulose (BNC) (Nguyen et al., 2021). Nanocellulose had good heavy metal adsorption capacity because of its large surface area around 150 $m^2 \cdot g^{-1}$ (Kaboorani and Riedl, 2015), it could be combined with other materials to improve recovery. In this project, nanocellulose would combine with ferromagnetic oxides, since the combination had some outstanding properties such as their ability to exhibit superparamagnetic properties with high saturation magnetization in the presence of an external magnetic field as well as their high surface area due to their size, compact size, good compatibility, low toxicity, and good physicochemical properties, and stability (Mustapić et al., 2016). With great dispersion in water, suspended suspension of nanocellulose powder could adsorb Lead well and materials combined with Fe_3O_4 would solve the problem of separating adsorbent from solution by the simple method of magnetic field. It could be easier to apply heavy metal and dyes handling expand to the world. In the experiment, the CNC/Fe_3O_4 materials synthesized by the in-situ method ensured that the properties of the component materials (CNC, Fe_3O_4 nanoparticle) did not change, increasing the ability to absorb lead ions with low content in water.

2. Materials and methods

2.1 Materials and chemicals

The Nanografi Company provided the cellulose nanocrystals used in this research, which had a diameter of 10 - 20 nm and a length of 300 - 900 nm. For in-situ synthesis of iron oxide, ammonium hydroxide 25 wt% (GHTech), ferric (III) chloride hexahydrate 99 % (Xilong Scientific), and ferrous (II) chloride 97 % (Xilong Scientific) were used in this study; and materials for wastewater: Lead (II) nitrate % (Xilong Scientific) was used as received. In all of the experiments, deionized (DI) water was utilized.

2.2 Synthesis of CNC/Fe$_3$O$_4$

The CNC/Fe$_3$O$_4$ was synthesized using the in-situ method with different CNC/Fe$_3$O$_4$ molar ratios. The cellulose nanocrystals (CNC) were first thoroughly dispersed in deionized water for 30 min in an ultrasonic bath. 1.2 g FeCl$_3$.6H$_2$O was added to the aforementioned suspension and agitated for one hour on the induction hob, followed by the addition of 0.45 g FeCl$_2$.4H$_2$O to the reaction mixture, which was then stirred for another hour under the argon flow at room temperature to obtain a bright yellow solution. After that, the ammonium hydroxide solution was gradually added to the dispersion. The reaction was maintained for an hour. When the reaction was completed, ferromagnetic oxide particles were formed, and the mixture's color changed to black. The magnetic cellulose nanocrystals (MCNC) were washed several times with water and ethanol using a centrifuge at 15,000 rpm for 15 min to pH = 7, finally dried in a vacuum oven at 85 °C for one hour. The concentration of CNC in each sample was kept constant at 0.7 % w/v nanocellulose crystal in DI, while the [Fe^{3+}]/[Fe^{2+}] molar ratio was kept constant at 2. The molar ratios of each sample CNC/Fe$_3$O$_4$ were 0.5:1; 1:1; 1.5:1; 2:1 and used to make samples 1 - 4. All of the experiments were maintained constant at 25 °C.
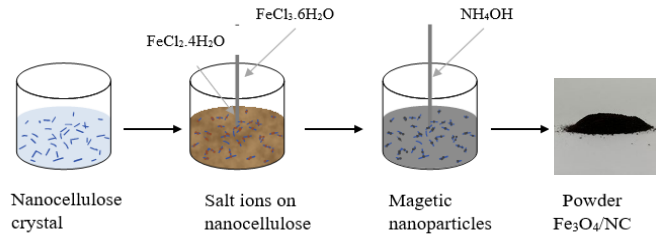
Figure 1: Preparation of magnetic crystal nanocellulose

2.3 Investigate the effect of initial Pb^{2+} concentration on the adsorption capacity of the material

Adsorption should be done as follows: weigh 0.05 g CNC/Fe$_3$O$_4$ into 50 mL Pb^{2+} ion solution which has been adjusted to pH = 5.5 – 6. The adsorption process took one hour. A magnet was used to extract CNC/Fe$_3$O$_4$ from the solution after that. The concentration of Pb^{2+} in the aqueous solution was measured using the inductively coupled plasma atomic emission spectroscopy (ICP-OES) technique after treatment. The Langmuir and Freundlich isotherm models, which were typically used to describe aqueous phase adsorption, were utilized to assess the experimental adsorption equilibrium data for Pb(II) on CNC/Fe$_3$O$_4$ (Jazi et al., 2014). The Langmuir isotherm model assumes that the adsorption of ions occurs on a homogeneous surface of the material and that the adsorption is monolayer, without any interaction between the adsorbed ions. The Freundlich isotherm model is an empirical equation based on the adsorption on the heterogeneous surface of the material and the adsorption is multilayer. Eq(1) and Eq(2) were used to express the Langmuir and Freundlich adsorption isotherms. The adsorption capacity (q$_e$) of Pb^{2+} onto the MCNC was calculated using the Eq(3).

$$\frac{C_e}{q_e} = \frac{1}{b.q_{max}} + \frac{C_e}{q_{max}} \tag{1}$$

$$\log q_e = \log K_F + \frac{1}{n}.\log C_e \tag{2}$$

$$q_e = (C_0 - C_e).V/m \tag{3}$$

where q$_{max}$ was the maximum adsorption capacity per gram of adsorbent (mg/g) and b was Langmuir's constant (L/mg), related to the adsorption energy. The Langmuir parameters were calculated from the slope and intersection of the C$_e$/q$_e$ versus q$_e$ linear graph (K$_F$ and n were the experimental constants of the Freundlich model for adsorption capacity and strength), and can be calculated from the slopes and intersections of the

linear graph. C_0 and C_e (mg/L) were the initial and equilibrium concentration of Pb^{2+}, m (g) is the weight of the hydrogel, and V (L) is the volume of Pb^{2+} solution (Neto et al., 2013).

2.4 Analytical indicators

X-ray diffraction (XRD) method was applied to analyze the crystal structure properties of the material. The B8 Bruker Advance instrument (Germany) used monochromatic Cu-Kα rays (λ = 1.5406 Å), voltage of 40 kV, current strength of 25 mA, scanning step of 0.02°, the speed of 0.25 s/step and scanning angle of 2θ ranging from 5 to 75°, measured at Biomass Laboratory.

Functional groups spectrum was measured using Fourier Transform Infrared (FT-IR). The samples were dried at 105 °C for 4 - 5 h, mixed with KBr, and vacuum pressed to form pellets. The FT-IR spectra of the samples were recorded in the transmission mode in the range 4,000 - 400 cm^{-1}. The results were measured on a BRUKER TENSOR 27, Germany at the Institute of Chemical Technology in Ho Chi Minh City.

The surface morphology of the nanoparticle was examined by Scanning Electron Microscopy (SEM). The image displayed the surface morphology of nanocellulose/ Fe_3O_4 nanoparticles and nanocrystals captured at various magnifications. The image was measured using the JSM-IT200 instrument at Ho Chi Minh University of Natural Resources and Environment.

Transmission electron microscopy (TEM) was used to image the material's structural morphology. The image was taken on the JEM1010-JEOL TEM machine of the Ultrastructural Laboratory at the Central Institute of Hygiene and Epidemiology, Hanoi. The sample was dispersed in water at a concentration of 0.5 mg/mL H_2O.

ICP-OES measurement method: measured on an Optima Emission Spectrometer 4300DV, at the Center for Analysis and Experimentation Services (CASE) in Ho Chi Minh City.

3. Result and discussion

3.1 Characterization of CNC/Fe₃O₄ nanocomposite

The XRD diffraction pattern analysis results for the CNC/Fe_3O_4 samples were shown in Figure 2. The XRD patterns of cellulose nanocrystals attached with iron oxide have six distinct peaks 2θ = 30.15°, 36.27°, 43.32°, 53.89°, 57.13°, and 62.29°, which were assigned to the crystallographic planes (220), (311), (400), (422), (511), and (440) correspond to the crystalline iron oxide structure (Liu et al., 2015). The peak at about 2θ = 22.6° was assigned to the (002) crystal plane, which correlated with the typical cellulose I polymorphism and can be seen in all samples, albeit with different intensities though. The high signal of Fe_3O_4 may have lowered the intensity of this peak. This demonstrates that Fe_3O_4 was successfully synthesized on the CNC surface, and the crystal structure of cellulose was preserved, as proven by the FTIR results.
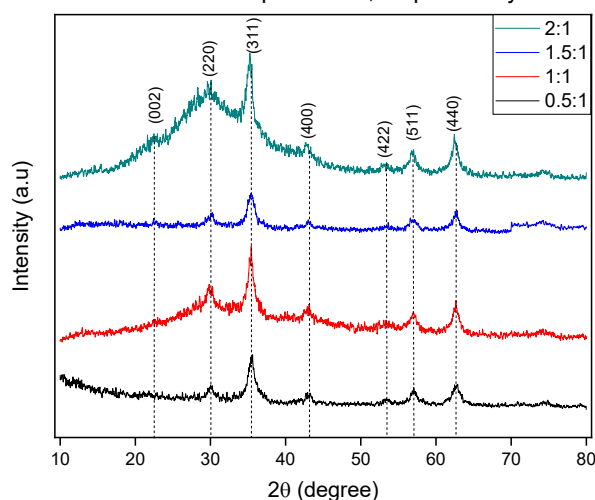
Figure 2: XRD diagram of CNC/Fe₃O₄ with different molar ratios

FTIR was used to characterize the structures of the produced materials. Figure 3 displayed the FTIR results of MCNC powder with a spectral pattern at 3,492.30 cm^{-1}, which was typical of stretching vibrations of hydroxyl groups (-OH) in intramolecular cellulose. C-H stretching vibrations were represented by the transmittance bands at 2,952.11 cm^{-1} and 2,833.47 cm^{-1}. The band at 1,390.74 cm^{-1} was assumed to be a reduced symmetry CH_2 oscillation. The transmittance bands were visible in the CNC sample. The Fe-O bond oscillation zone developed with modest strength around the 410 cm^{-1} peak, as illustrated in Figure 3 (Amiralian et al., 2020). There was no

peak near 632 cm^{-1} was proof that the Fe$_2$O$_3$ phase did not exist in the samples. As a result, the obtained particles were mostly Fe$_3$O$_4$. The high-intensity band at 568 cm^{-1} in the MCNC spectrum corresponded to the Fe-O stretching vibrations and was specific to Fe$_3$O$_4$. This peak indicated that Fe$_3$O$_4$ nanoparticles were successfully formed on the nanocellulose surface (Ozmen et al., 2010). The hydroxyl groups on CNC's surface provided a high loading capacity for metal ions. All additional CNC transmission peaks were kept in the MCNC samples, demonstrating that the CNC component was preserved after the Fe$_3$O$_4$ nanoparticles were synthesized.
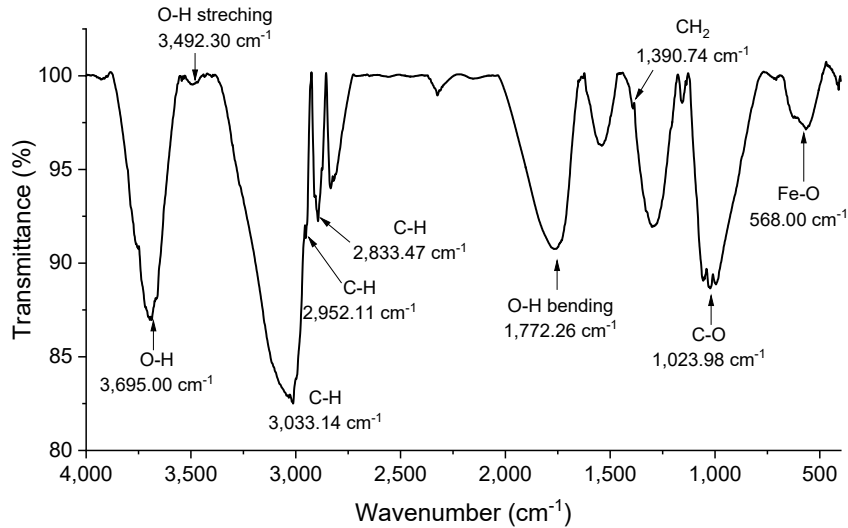
Figure 3: FTIR spectrum of CNC/Fe$_3$O$_4$

Figure 4 showed SEM images of CNC/Fe$_3$O$_4$ materials from samples 1 - 4 with different CNC/Fe$_3$O$_4$ ratios, demonstrating that Fe$_3$O$_4$ had a spherical shape with a size of around 5 - 15 nm and cellulose nanocrystals had a length of 250 - 300 nm and a diameter of 20 - 30 nm. The material had the most consistent distribution between CNC and Fe$_3$O$_4$ according to the picture above with a ratio of 1:1. The combination of Fe$_3$O$_4$ and CNC could be explained based on the electrostatic bonding of Fe$_3$O$_4$ particles with the hydroxyl (–OH) and epoxy (–O–) functional groups of CNC. Thanks to these bonds, it helped to immobilize or intercalate Fe$_3$O$_4$ particles with cellulose nanoparticles (Lei et al., 2014).
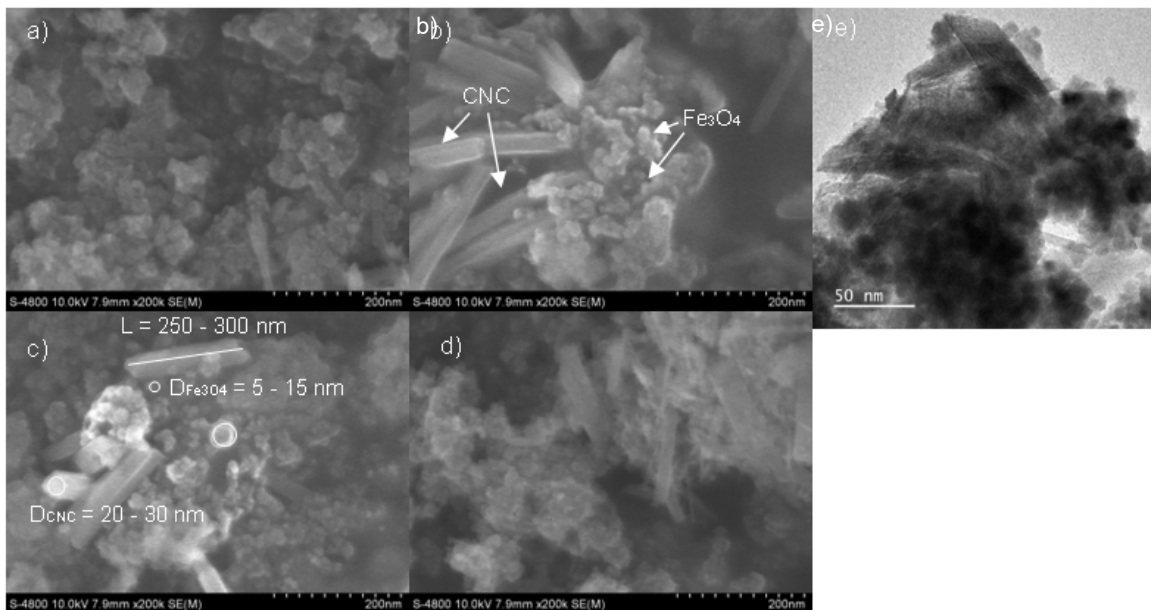
Figure 4: SEM images of CNC/Fe$_3$O$_4$ with the ratios (a) 0.5:1, (b) 1:1, (c) 1.5:1, (d) 2:1, (e) TEM image of CNC/Fe$_3$O$_4$

Figure 4e presented TEM images of CNC/Fe_3O_4 materials, showing that Fe_3O_4 had a spherical shape with a size of about 10 - 15 nm. The TEM image also showed that the striped particle arrays were cellulose crystal nanoparticles, scattered ferromagnetic particles interspersed with CNC particles. The ferromagnetic particles agglomerated quite a lot, masking the shape of the CNC, so the spread was low, there were many places with denser density. The background material (CNC) and filler material could still be seen clearly (Fe_3O_4). The nanoparticle size distribution was less uniform. The main reason lied in the process of nucleation and sprouting into nanoparticles. When the concentration of Fe_3O_4 molecules reached the critical saturation state, nucleation occurred, after which the sprout grew into nanoparticles through the diffusion of Fe_3O_4 molecules onto the surface of the germ. The main reason for the formation of nanoparticles of less uniform size was believed to be the fast reaction rate and therefore the number of new nuclei formed in parallel with the sprout development. The sprouts formed at an early stage will grow into nanoparticles that were larger in size than those formed from those formed at a later stage (Faraji et al., 2010).

3.2 Effect of the initial concentration of Pb^{2+} on the adsorption capacity of the material

Investigation of the adsorption process of Pb^{2+} in water at a concentration of 200 ppm by CNC/Fe_3O_4 in the period from 10 to 120 minutes. The results obtained adsorption reached equilibrium after 1 hour (Figure 5a). With the same Pb^{2+} concentration in water of 200 ppm, samples with different CNC/Fe_3O_4 molar ratios gave adsorption results as shown in Table 1.

Table 1: Table result of the effect of CNC/Fe_3O_4 molar ratio on the adsorption

Molar ratio of CNC/Fe_3O_4	0.5:1	1:1	1.5:1	2:1
C_o (mg/L)	200	200	200	200
C_e (mg/L)	89.3	86.8	88.0	87.7
q_e (mg/L)	110.7	113.2	112	112.3

After adsorption with the same concentration of Pb^{2+} in each sample, the concentration of Pb^{2+} in the sample according to the 1:1 molar ratio was the smallest corresponding to the CNC/Fe_3O_4 material being adsorbed the most. The results can be interpreted together with the results of the XRD and SEM images. Because of this 1:1 ratio, Fe_3O_4 and CNC particles had the most uniformly distributed structure, so the adsorption capacity of Pb^{2+} was higher than the remaining ratios recorded in Table 1. With the ratio determined as above, compared with the change in the concentration of Pb^{2+} in water, the adsorption will follow the isothermal adsorption model.
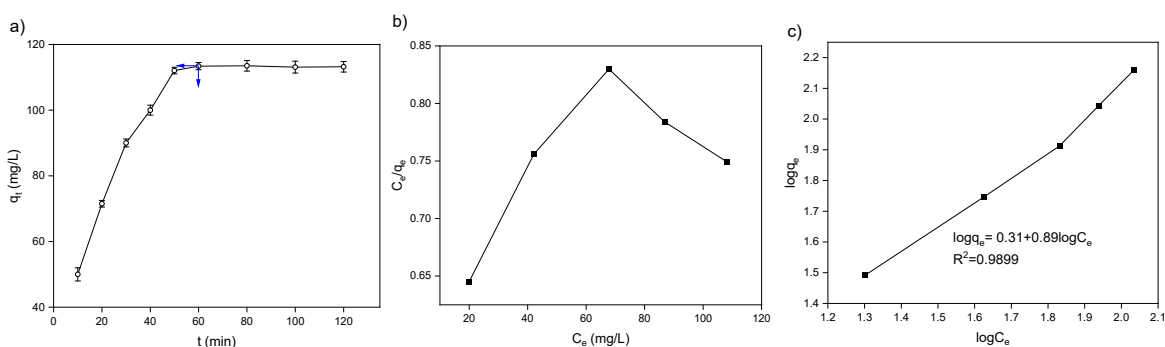
Figure 5: (a) Lead adsorption capacity follow time and isothermal model adsorption equation according to (b) Langmuir, and (c) Freundlich

The isotherm parameters of the two models for Pb^{2+} adsorption by the MCNC can be evaluated via the slopes and intercepts of the linear plots of C_e/q_e versus C_e for the Langmuir model (Figure 5b) and log C_e versus log q_e versus for the Freundlich model (Figure 5c). The calculated maximum adsorption capacity (q_{max}) of the MCNC toward Pb^{2+} from the Langmuir model is 241.6 mg/g, which is larger than the experimental value (112 mg/g). Compared with the correlation coefficient of the Langmuir model ($R^2 = 0.33813$), the R^2 value of the Freundlich model ($R^2 = 0.9899$) is higher. The Freundlich isotherm model matches better with the adsorption behavior with parameters $K_F = 2.04$, n = 1.12. Pb^{2+} adsorption onto the MCNC occurs mainly on the heterogeneous surface or surface support positions with different affinities. The Freundlich constant n is larger than 1, indicating the high adsorption intensity of the MCNC toward Pb^{2+} (Peng et al., 2022). This is a multilayer adsorbent material. Because Fe_3O_4 as well as CNC have the ability to adsorb lead (Lu et al., 2016). These two materials can still form nano-sized multilayer adsorbents when they are co-precipitated, and this is demonstrated by the regression

coefficient $R^2 = 0.9899$, which is compatible with the hypothesis of the multilayer structure of the Freundlich isotherm adsorption equation.

4. Conclusions

Cellulose nanocrystals were used to synthesize magnetic cellulosic nano-composite with the average Fe_3O_4 particle diameter of less than 15 nm using a simple co-precipitation method. The optimization study also suggested that the appropriate molar ratio for the two materials (CNC/Fe_3O_4) was 1:1. The synthesized material can be used as an absorbent for Pb^{2+} in contaminated water. The absorption capacity at time balance (q_e) was 0.1132 mg/g. The lead adsorption process followed a Freundlich isotherm adsorption model ($R^2 = 0.9899$). This nanocomposite material could find further application in waste water treatment due to its positive efficiency.

Acknowledgments

References

Amiralian N., Mustapic M., Hossain M.S.A., Wang C., Konarova M., Tang J., Na J., Khan A., Rowan A., 2020, Magnetic nanocellulose: A potential material for removal of dye from water, Journal of Hazardous Materials, 394.

Faraji M., Yamini Y., Rezaee M., 2010, Magnetic nanoparticles: Synthesis, stabilization, functionalization, characterization, and applications, Journal of the Iranian Chemical Society, 7(1), 1–37.

Jazi M.B., Arshadi M., Amiri M.J., Gil A., 2014, Kinetic and thermodynamic investigations of Pb (II) and Cd (II) adsorption on nanoscale organo-functionalized SiO_2-Al_2O_3, Journal of Colloid and Interface Science, 422, 16–24.

Kaboorani A., Riedl B., 2015, Surface modification of cellulose nanocrystals (CNC) by a cationic surfactant, Industrial Crops and Products, 65, 45-55.

Khalil H.A., Bhat A.H., Yusra A.I., 2012, Green composites from sustainable cellulose nanofibrils: A review, Carbohydrate polymers, 87(2), 963-979.

Lei Y., Chen F., Luo Y., Zhang L., 2014, Three-dimensional magnetic graphene oxide foam/Fe_3O_4 nanocomposite as an efficient absorbent for Cr (VI) removal, Journal of Materials Science, 49(12), 4236–4245.

Liu K., Nasrallah J., Chen L., Huang L., Ni Y., 2015, Preparation of CNC-dispersed Fe_3O_4 nanoparticles and their application in conductive paper, Carbohydrate Polymers, 126, 175-178.

Lu J., Jin R.N., Liu C., Wang Y.F., Ouyang X.K., 2016, Magnetic carboxylated cellulose nanocrystals as adsorbent for the removal of Pb(II) from aqueous solution, International Journal of Biological Macromolecules, 93, 547-556.

Mustapić M., Al Hossain M.S., Horvat J., Wagner P., Mitchell D.R., Kim J.H., Alici G., Nakayama Y., Martinac B., 2016, Controlled delivery of drugs adsorbed onto porous Fe_3O_4 structures by application of AC/DC magnetic fields, Microporous and Mesoporous Materials, 226, 243-250.

Neto V.D.O.S., Raulino G.S.C., Paulo de Tarso C.F., Araújo-Silva M.A., Nascimento R.F., 2013, Equilibrium and kinetic studies in adsorption of toxic metal ions for wastewater treatment, Viewpoints, 7, 8.

Nguyen C.T.X., Bui K.H., Truong B.Y., Do N.H.N., Le P.T.K., 2021, Nanocellulose from pineapple leaf and its applications towards high-value engineering materials, Chemical Engineering Transactions, 89, 19-24.

Ozmen M., Can K., Arslan G., Tor A., Cengeloglu Y., Ersoz M., 2010, Adsorption of Cu(II) from aqueous solution by using modified Fe_3O_4 magnetic nanoparticles, Desalination, 254(1-3), 162-169.

Shen J.M., Tang W.J., Zhang X.L., Chen T., Zhang H.X., 2012, A novel carboxymethyl chitosan-based folate/Fe_3O_4/CdTe nanoparticle for targeted drug delivery and cell imaging, Carbohydrate Polymers, 88(1), 239–249.

Peng Z., Yu H.R., Wen J.Y., Wang Y.L., Liang T., Cheng C.J., 2022, A novel ion-responsive photonic hydrogelsensor for portable visual detection and timely removal of lead ions in water, Materials Advances, 3, 5393-5405.